

# Robust Weak Measurements with Certified Single Photons

Enrico Rebufello, Fabrizio Piacentini,\* Alessio Avella, Muriel A. de Souza, Marco Gramegna, Rudi Lussana, Federica Villa, Jan Dziewior, Eliahu Cohen, Lev Vaidman, Ivo Pietro Degiovanni, and Marco Genovese

Since their introduction, weak measurements and weak values have served as a cornerstone for investigating quantum measurement theory, as well as a significant tool for quantum metrology and sensing. Here, it is shown how (anomalous) weak values can be reliably obtained with single quantum systems even without averaging over multiple experimental runs, thanks to a measurement protocol dubbed *robust weak measurement*. Specifically, robust weak measurements are exploited to extract the weak value of the polarization of heralded single photons, certifying the true single-particle, nonclassical nature of weak values.

protocol dubbed *robust weak measurement* (RWM) was recently introduced and experimentally demonstrated.<sup>[73]</sup> This protocol allows extracting (anomalous) WVs with relatively small uncertainty even from just a single reading of our measurement device, i.e., without the averaging process. In ref. [73] the experiment was run with a multi-thermal light source attenuated at the single photon level and detected, after the RWM process, by an Electron Multiplying Charge-Coupled Device (EM-CCD);<sup>[74]</sup> therefore, although we demonstrated

## 1. Introduction

Even after 36 years since their introduction by Aharonov, Albert and Vaidman (AAV),<sup>[1]</sup> weak measurements (WMs), and weak values (WVs)<sup>[2]</sup> represent one of the most intriguing and debated quantum measurement paradigms, with many experimental applications ranging from foundations of quantum mechanics<sup>[3–27]</sup> to quantum metrology and other quantum technologies.<sup>[28–53]</sup> Nevertheless, WMs and WVs still remain a controversial topic,<sup>[54–72]</sup> both for what concerns their interpretation and the quantumness of their very nature. To operationally address this matter, a novel weak-interaction-based

the possibility of reliably extracting a (anomalous) WV with a single click of our detector, one could still argue that this could not be strictly considered a single-particle experiment, since the source exploited didn't emit properly certified single particles (e.g., heralded single photons).

In this article, besides illustrating in detail the analysis that allowed us to obtain the results in ref. [73], we address this single-particle issue by presenting further results obtained by implementing a RWM on single photons emitted by a heralded photon source based on spontaneous parametric down-conversion (SPDC), confirming the extraordinary measurement capability shown in ref. [73] and overcoming the aforementioned criticism.

E. Rebufello, F. Piacentini, A. Avella, M. Gramegna, I. P. Degiovanni, M. Genovese

INRIM - Istituto Nazionale di Ricerca Metrologica  
strada delle Cacce, Torino 91 10135, Italy  
E-mail: [f.piacentini@inrim.it](mailto:f.piacentini@inrim.it)

M. A. de Souza  
National Institute of Metrology  
Quality and Technology—INMETRO  
Av. Nossa Senhora das Graças, 50, Duque de Caxias RJ 25250-020, Brazil

R. Lussana, F. Villa  
Politecnico di Milano  
Dipartimento di Elettronica  
Informazione e Bioingegneria  
Piazza Leonardo da Vinci 32, Milano 20133, Italy

J. Dziewior  
Max-Planck-Institut für Quantenoptik  
Hans-Kopfermann-Straße 1, 85748 Garching, Germany

J. Dziewior  
Department für Physik  
Ludwig-Maximilians-Universität  
80797 München, Germany

E. Cohen  
Faculty of Engineering and the Institute of Nanotechnology and  
Advanced Materials  
Bar Ilan University  
Ramat Gan 5290002, Israel

L. Vaidman  
School of Physics and Astronomy  
Tel-Aviv University  
Tel-Aviv 69978, Israel

L. Vaidman  
Institute for Quantum Studies  
Chapman University  
Orange, CA 92866, USA

I. P. Degiovanni, M. Genovese  
INFN  
sede di Torino  
via P. Giuria 1, Torino 10125, Italy

 The ORCID identification number(s) for the author(s) of this article can be found under <https://doi.org/10.1002/qute.202400482>

© 2025 The Author(s). Advanced Quantum Technologies published by Wiley-VCH GmbH. This is an open access article under the terms of the [Creative Commons Attribution](#) License, which permits use, distribution and reproduction in any medium, provided the original work is properly cited.

DOI: 10.1002/qute.202400482

Taking into account the advantage granted by the heralding process in terms of technical noise (i.e., dark counts on our detection system) reduction, our results might foster novel techniques for quantum sensing, quantum metrology and other quantum technologies.

## 2. Theoretical Framework

The WV of an observable  $\hat{A}$  was defined as the reading of a standard von Neumann measuring procedure with weakened coupling.<sup>[1]</sup> The von Neumann measurement interaction Hamiltonian is

$$\hat{H}_{\text{int}} = g(t)\hat{A} \otimes \hat{P} \quad (1)$$

with  $\int g(t)dt = 1$ , where  $g(t)$  is well localized and shows the time of the measurement, i.e. the time interval in which the coupling between quantum system and measuring device occurs. The weakness of the coupling is achieved by arranging a special initial state of the measuring device presenting  $\langle \hat{P} \rangle = 0$  and  $\Delta \hat{P}$  very small, and therefore very large uncertainty of the pointer variable  $\hat{Q}$ . Of course, in such a procedure, one reading of the measuring device will tell us almost nothing, but given an ensemble of identical experiments with the same preparation and the same postselection (the WVs are of interest when the postselection is involved, otherwise these are just expectation values) the average will converge to a particular value. Given that between pre and postselection other interactions can be neglected and our measuring interaction vanishes at the limit, the reading will be given by the AAV formula:

$$\langle \hat{A} \rangle_w^{(AAV)} = \frac{\langle \psi_\beta | \hat{A} | \psi_\alpha \rangle}{\langle \psi_\beta | \psi_\alpha \rangle} \quad (2)$$

where  $|\psi_\alpha\rangle$  and  $|\psi_\beta\rangle$  are, respectively, the pre- and postselected quantum states.

Observation of the WV using the weak interaction of Equation (1) requires an ensemble, because “vanishing measurement interaction” requires huge uncertainty of the pointer variable before and after the measurement. This feature led to a controversy regarding the interpretation of WVs.<sup>[18,54–72]</sup>

Here we consider a single-run experiment which extracts WVs with a reasonable precision. Our measurement coupling has the same form as in Equation (1), but it is not vanishingly small, so it cannot be neglected. It is no longer true that, between pre- and postselection, the system is described by the states  $|\psi_\alpha\rangle$  and  $|\psi_\beta\rangle$ , so the WV expression in Equation (2) has to be modified.<sup>[75]</sup>

The definition of WV as the outcome of weak (with vanishingly small interaction) measurement remains the same, but due to our measurement interaction the system at intermediate times becomes entangled with our measuring device, and described by evolving mixed states. Fortunately, interactions of the form of Equation (1) keep the WV of  $\hat{A}$  unchanged during the period of measurement, so there is one particular WV during the whole period which we find in our procedure. Of course, the expression for this WV is not the one in Equation (2), but it is derived for mixed states in ref. [37], where it is also shown that the expectation value of the Gaussian meter shows the real part of the WV. Since the

WV does not change during the measurement, we can take any moment for its calculation, and the easiest choice is the moment just before postselection. The Hamiltonian in Equation (1) generates the time evolution  $\hat{U} = \exp(-i \int \hat{H}_{\text{int}} dt) = \exp(-i\hat{A} \otimes \hat{P})$ , acting on the quantum system in the preselected state  $|\psi_\alpha\rangle$ , obtained by applying the projector  $\hat{\Pi}_\alpha = |\psi_\alpha\rangle\langle\psi_\alpha|$ . After the unitary evolution, postselection onto the final state  $|\psi_\beta\rangle$  is realized by the projector  $\hat{\Pi}_\beta = |\psi_\beta\rangle\langle\psi_\beta|$ . At the end of the measurement process, the final read-out allowing to extract the information about the WV is made via the measurement device meter observable  $\hat{Q}$ , canonically conjugated to the pointer  $\hat{P}$ . For a Gaussian meter  $|\varphi(q)\rangle = \int dqf(q)|q\rangle$ , with  $f(q) = \frac{1}{\sqrt{\sigma\sqrt{2\pi}}} \exp\left(-\frac{q^2}{4\sigma^2}\right)$ , and a weak coupling regime granted by a large meter uncertainty (i.e.,  $\Delta q = \sigma \gg 1$ ), the WV information takes the form of a shift in  $q$ , i.e., the meter state after the WM will be  $|\varphi(q - \langle \hat{A} \rangle_w)\rangle$ .

From now on, let us consider a scenario in which we want to measure the polarization  $\hat{A} = |H\rangle\langle H| - |V\rangle\langle V|$  of a photon, where  $H$  ( $V$ ) the horizontal (vertical) polarization component, preselected in the state  $|\psi_\alpha\rangle = \cos\alpha|H\rangle + \sin\alpha|V\rangle$  and postselected in the state  $|\psi_\beta\rangle = \cos\beta|H\rangle + \sin\beta|V\rangle$ . The AAV formula of WV given by Equation (2) corresponds to a limit of the weak regime ( $\sigma \gg 1$ ), i.e., when entanglement between the pointer and measured observable states can be neglected. For a large but finite  $\sigma$ , the von Neumann coupling between the polarization and the pointer leads to the following evolution:

$$|\psi_\alpha\rangle \otimes |\varphi(q)\rangle \xrightarrow{\hat{U}} \cos\alpha|H\rangle|\varphi(q-1)\rangle + \sin\alpha|V\rangle|\varphi(q+1)\rangle \quad (3)$$

The photon polarization degree of freedom ends up in a mixed polarization state described by the density matrix:

$$\rho_\alpha = \begin{pmatrix} \cos^2\alpha & e^{-\frac{1}{2\sigma^2}} \sin\alpha \cos\alpha \\ e^{-\frac{1}{2\sigma^2}} \sin\alpha \cos\alpha & \sin^2\alpha \end{pmatrix} \quad (4)$$

For mixed states, the AAV formula in Equation (2), holding for pure states, is generalized in Equation (32) of ref. [75]. Given the postselection onto  $\rho_\beta = |\psi_\beta\rangle\langle\psi_\beta|$ , our WV becomes:

$$\langle \hat{A} \rangle_w = \frac{\text{tr}(|\psi_\beta\rangle\langle\psi_\beta| \hat{A} \rho_\alpha)}{\text{tr}(|\psi_\beta\rangle\langle\psi_\beta| \rho_\alpha)} = \frac{Z_H^2 - Z_V^2}{Z_H^2 + Z_V^2 + 2Z_H Z_V e^{-\frac{1}{2\sigma^2}}} \quad (5)$$

where  $Z_H = \langle \psi_\beta | \hat{\Pi}_H | \psi_\alpha \rangle = \cos\alpha \cos\beta$  and  $Z_V = \langle \psi_\beta | \hat{\Pi}_V | \psi_\alpha \rangle = \sin\alpha \sin\beta$ . This formula, taking into account the effective coupling intensity in the von Neumann interaction between the pre- and postselection processes, converges to the AAV one in Equation (2) in the limit  $\sigma \rightarrow \infty$ . Note that Equation (5) does not constitute a new definition of WV. Indeed, the WV is obtained by the measurement of a weakly-coupled measuring device; such a coupling performed between pre- and postselection will yield the value provided by Equation (5).

Consider now a quantum system  $S$  composed of  $N$  particles, and suppose we want to measure the total system variable:

$$\hat{A}^S = \frac{1}{N} \sum_{k=1}^N \hat{A}_k \quad (6)$$

where  $\hat{A}_k$  corresponds to the variable pertaining the  $k$ -th particle. Within the standard WV framework, in which each particle has its own measuring device, the uncertainty of measuring  $\hat{A}^S$  would scale like  $\sqrt{N}$ , due to the contribution of  $N$  measurement devices. In RWM (originally introduced in ref. [76], the paper submitted in parallel with the invention of WVs<sup>[1]</sup>), instead, all the  $N$  systems are coupled with a single measurement device, thus avoiding the  $\sqrt{N}$  increase. This difference in scaling is crucial, allowing to extract an anomalous WV  $\langle \hat{A}^S \rangle_w$  even by a single click of the measuring device.<sup>[73]</sup>

In our case, we consider the (normalized) sum of the polarization observables of  $N$  photons collectively preselected in the state  $|\psi_\alpha^{(N)}\rangle = \otimes_{k=1}^N |\psi_\alpha^{(k)}\rangle$  and postselected in the state  $|\psi_\beta^{(N)}\rangle = \otimes_{k=1}^N |\psi_\beta^{(k)}\rangle$ , coupled to the same measuring device by means of the interaction Hamiltonian

$$\hat{H}_{\text{int}} = g(t) \left( \sum_{k=1}^N \hat{A}_k \right) \otimes \hat{P} \quad (7)$$

in which a temporally well-localized  $g(t)$  defines the time interval during which the measurement occurs. As per traditional WMs, the pointer  $\hat{P}$  is canonically conjugated to the meter  $\hat{Q}$ , initialized in the state  $|\varphi(q)\rangle$  defined above.

Looking back at the interaction Hamiltonian  $\hat{H}_{\text{int}} = g(t) \left( \sum_{k=1}^N \hat{A}_k \right) \otimes \hat{P}$ , we notice that the observables  $\hat{A}_k$  are constants of motion, hence the time in which each interaction takes place does not matter. This allows us to switch to a different scenario, in which we use only *one* photon (instead of  $N$ ) and realize pre-selection, interaction and postselection  $N$  times on it.<sup>[73]</sup> Such a framework permits an alternative description of RWM as an iterative protocol consisting of  $N$  “interaction blocks”, modeled by the operator  $\hat{\mathcal{W}}$  and composed of a pre-selection on the state  $|\psi_\alpha\rangle$  followed by a weak interaction  $\hat{U}$  and a postselection on the state  $|\psi_\beta\rangle$ , plus a rotation operator  $\hat{R} = |\psi_\alpha\rangle\langle\psi_\beta|$  transforming  $|\psi_\beta\rangle$  into  $|\psi_\alpha\rangle$  to avoid pre-selection losses between subsequent blocks:

$$\hat{\mathcal{W}} = \hat{R} \hat{\Pi}_\beta \hat{U} \hat{\Pi}_\alpha \quad (8)$$

Naively, one may expect each block to shift the pointer proportionally to the WV given by Equation (2), but non-ideal couplings have been shown to affect the state evolution<sup>[36,37]</sup> (especially for strong anomalous values), resulting in the reduction of the anomalous trait of the WV. At the end of the entire protocol the spatial state is shifted:  $|\varphi(q - N\langle \hat{A} \rangle_w)\rangle$ , where the WV is given by Equation (5). Indeed, after  $N$  steps, the initial state  $|\Psi_{\text{in}}\rangle = |\psi_\alpha\rangle \otimes |\varphi(q)\rangle$  evolves into the state

$$\begin{aligned} |\Psi_{\text{out}}\rangle &= C^{-1} \hat{\mathcal{W}}^N |\Psi_{\text{in}}\rangle = C^{-1} (\hat{R} \hat{\Pi}_\beta \hat{U} \hat{\Pi}_\alpha)^N |\psi_\alpha\rangle \otimes |\varphi(q)\rangle \\ &= C^{-1} \sum_k \binom{N}{k} Z_H^k e^{-ik\hat{P}} Z_V^{N-k} e^{+i(N-k)\hat{P}} |\psi_\alpha\rangle \otimes |\varphi(q)\rangle \end{aligned} \quad (9)$$

with  $C$  playing the role of a normalization coefficient. We can then write the probability density function related to the photon

being in the position  $q_0$  after the  $N$ -step RWM as:

$$\begin{aligned} P_N(q_0|\alpha, \beta, N) &= C^{-2} |\langle q_0 | \otimes \langle \psi_\alpha | | \Psi_{\text{out}} \rangle|^2 \\ &= C^{-2} \left| \sum_{k=0}^N \binom{N}{k} Z_H^k Z_V^{N-k} f(q_0 - (2k - N)) \right|^2 \end{aligned} \quad (10)$$

By integrating Equation (10) over  $q_0$  and requiring  $\int dq_0 P_N(q_0|\alpha, \beta, N) = 1$ , we obtain:

$$C^2 = \sum_{k=0}^N \sum_{k'=0}^N \binom{N}{k} \binom{N}{k'} Z_H^{k+k'} Z_V^{2N-k-k'} \exp\left[-\frac{1}{2\sigma^2}(k-k')^2\right] \quad (11)$$

We underline that  $C^2$  corresponds to the probability of a single photon to survive the  $N$ -step RWM. The meter position expectation value can therefore be expressed as

$$\begin{aligned} \langle q \rangle &= \int dq q P_N(q|\alpha, \beta, N) = C^{-2} \sum_{k=0}^N \sum_{k'=0}^N \binom{N}{k} \binom{N}{k'} Z_H^{k+k'} Z_V^{2N-k-k'} \\ &\quad (N - k - k') \exp\left(-\frac{1}{2\sigma^2}(k - k')^2\right) \end{aligned} \quad (12)$$

while its standard deviation is  $\Delta_q = \sqrt{\langle q^2 \rangle - \langle q \rangle^2}$ , where

$$\begin{aligned} \langle q^2 \rangle &= C^{-2} \sum_{k=0}^N \sum_{k'=0}^N \binom{N}{k} \binom{N}{k'} Z_H^{k+k'} Z_V^{2N-k-k'} \\ &\quad \left( (N - k - k')^2 + \sigma^2 \right) \exp\left(-\frac{1}{2\sigma^2}(k - k')^2\right) \end{aligned} \quad (13)$$

Following Equations (6) and (7), the measured WV and the associated statistical uncertainty can be respectively estimated as:

$$\langle \hat{A}^S \rangle_w^{(m)} = \frac{\langle q \rangle}{N} \quad \Delta_{\langle \hat{A}^S \rangle_w^{(m)}} = \frac{\Delta_q}{N} \quad (14)$$

Equations (5) and (12) highlight how the RWM outcome shows a non-trivial dependence also on the number of steps (or particles)  $N$ , that has to be carefully considered when realizing the protocol (see Appendix A for further details).

To quantitatively estimate the RWM performances for different  $N$  values, one might choose, for all the cases, the same measurement resolution power  $R \equiv \frac{C}{\sigma}$  ( $\sigma \geq 1$ ), fixing  $G = \sum_{i=1}^N \int g_i^{(N)}(t) dt = M$  (being  $M = \text{Max}(N)$  the largest  $N$  value considered in the comparison). This means that the single-step interaction intensity  $\int g_i^{(N)}(t) dt = \frac{C}{N}$  grows larger as  $N$  decreases, resulting instead in a weaker system-device coupling per step for larger  $N$  and approaching the case of Equation (2) for  $N \gg 1$ . The results of this comparison are reported in **Figure 1a–c**, where we can observe how, for increasing  $N$ , the RWM outcome becomes closer to the full pre- and postselection WV in Equation (2). For large  $N$  values, this allows obtaining anomalous WVs with a much higher precision (i.e., smaller uncertainty) compared to traditional WM protocols.

Analogously, we can study how the extracted WV  $\langle \hat{A}^S \rangle_w^{(m)}$  changes by varying the pre- and postselection angles  $\alpha$  and  $\beta$

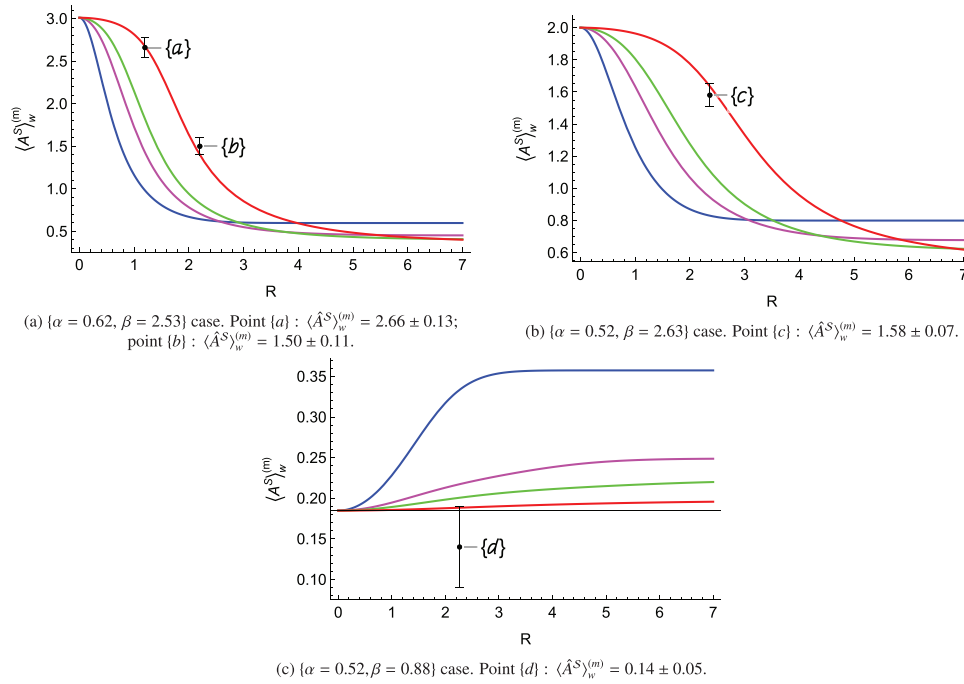


**Figure 1.** Plots (a–c): WV extracted by our RWM procedure for a fixed choice of  $\alpha$  and  $\beta$  (different for each plot) and different  $N$  values, considering the same measurement resolution power  $R \equiv \frac{C}{\sigma}$  ( $\sigma \geq 1$ ). To this purpose, we fix  $G = \sum_{i=1}^N \int g_i^{(N)}(t) dt = M$ , where  $M = \text{Max}(N)$  is the largest  $N$  value considered in the comparison, hence the single-step interaction intensity  $\int g_i^{(N)}(t) dt = \frac{C}{N}$  grows as  $N$  decreases. Blue line:  $N = 1$ . Magenta line:  $N = 2$ . Green line:  $N = 3$ . Red line:  $N = 7$ . Dots and uncertainty bars {a–d} correspond to the WVs given by the experimental results reported in ref. [73], obtained with different  $\alpha, \beta$  and  $\sigma$  values. The case of Equation (2), i.e., in the full pre- and postselection scenario where no entanglement is induced between system and pointer, is obtained for an infinitely wide Gaussian meter ( $\sigma \rightarrow \infty$ ), corresponding to  $R \rightarrow 0$ .

while keeping fixed the number of blocks  $N$  and the von Neumann interaction intensity, represented by the parameter  $\eta = \exp\left(-\frac{1}{2\sigma^2}\right)$  (with  $\eta \rightarrow 1$  corresponding to the case of full pre- and postselection for which AAV formula in Equation (2) holds).

To do this, in **Figure 2** we plot the expected WV  $\langle \hat{A}^S \rangle_w^{(m)}$  given by our  $N = 7$  steps RWM with respect to the full pre- and postselection one  $\langle \hat{A}^S \rangle_w = \langle \psi_\beta | \hat{A}^S | \psi_\alpha \rangle / \langle \psi_\beta | \psi_\alpha \rangle$  reported in Equation (2). We can then appreciate how, as the WV anomaly grows, the deviation from the case of complete pre- and postselection increases accordingly, with the  $\langle \hat{A}^S \rangle_w^{(m)} \simeq \langle \hat{A}^S \rangle_w$  region expanding as  $\eta$  approaches unity (i.e., for growing meter distribution width  $\sigma$ ). In the following, we will show how RWM allows obtaining anomalous WVs with relatively small uncertainty (much smaller than the ones granted by usual WM protocols) even in a single-particle experiment, by measuring the WV of the polarization of pre- and postselected certified single photons emitted by a heralded single-photon source.

### 3. RWM Experiment with Heralded Single Photons

In our setup (**Figure 3**), we generate heralded single photons by means of a mode-locked Ti:Sa laser with a second harmonic at 398 nm and a 76 MHz repetition rate, pumping a  $10 \times 10 \times 5$  mm LiIO<sub>3</sub> non-linear crystal in which Type-I spontaneous parametric down-conversion (SPDC) takes place, producing correlated photon pairs with one photon at 920 nm (called “idler”) and the other at 702 nm (dubbed “signal”). An interference filter (IF) centered

at 920 nm and with a 10 nm full width at half maximum (FWHM) filters the idler photon, which are then coupled to a single-mode fibre (SMF) and addressed to a Silicon single-photon avalanche diode (SPAD).

A click on this SPAD heralds the presence of the correlated signal photon on the other branch; this photon is filtered with a 702 nm centered IF with a 10 nm FWHM, SMF-coupled and addressed either to another Silicon SPAD or to the optical path in which the experiment is run. In the former case, we characterize our heralded single-photon source emission in terms of its second-order Glauber autocorrelation function  $g^{(2)}(t)$  that, for an ideal single-photon emission, should give  $g^{(2)}(0) = 0$ . With a metrological protocol analogous to the one introduced in ref. [77] we measured  $g^{(2)}(0) = 0.13 \pm 0.01$  (without any background or dark count subtraction), certifying the high quality of the single-photon state produced by our SPDC-based heralded photon source.

In the latter case (corresponding to the RWM implementation), the signal photon is decoupled, collimated in a Gaussian spatial mode with width  $\sigma$  and pre-selected in the polarization state  $|\psi_\alpha\rangle$  by a polarizing beam-splitter (PBS) followed by a half wave-plate (HWP).

Afterwards, the heralded single photons interact with  $N = 7$  interaction blocks realizing our RWM. Each block consists of two thin birefringent crystals (BCs), responsible for the time evolution  $\hat{U}$  realizing the von Neumann coupling between measured quantum system and measurement device, followed by a polarizer (Pol) realizing the postselection projector  $\hat{\Pi}_\beta$  (to re-

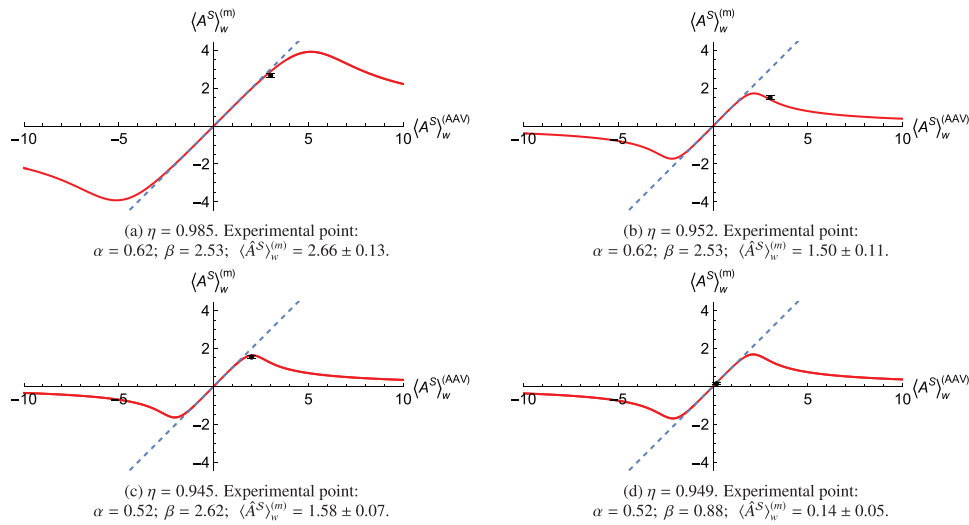


**Figure 2.** Discrepancy between  $\langle \hat{A}^S \rangle_w^{(m)}$  expected from a  $N = 7$  steps RWM protocol and the one corresponding to the full pre- and postselection case ( $\eta \rightarrow 1$ )  $\langle \hat{A}^S \rangle_w^{(AAV)} = \langle \psi_\beta | \hat{A}^S | \psi_\alpha \rangle / \langle \psi_\beta | \psi_\alpha \rangle$ , for four different  $\eta$  values and pre- and postselection angles  $\alpha$  and  $\beta$ . The dashed blue line represents the condition  $\langle \hat{A}^S \rangle_w^{(m)} = \langle \hat{A}^S \rangle_w^{(AAV)}$ , while the red continuous curve shows the RWM outcome behavior for  $\eta \lesssim 1$ . The black dots and bars represent, respectively, the experimental results and associated uncertainties obtained with our RWM procedure in ref. [73].

duce unwanted deviations due to the polarizer thickness we use thin polarizing plates) and a HWP used to rotate  $|\psi_\beta\rangle$  onto  $|\psi_\alpha\rangle$ , hence realizing the lossless pre-selection  $\hat{\Pi}_\alpha R$  for the subsequent step. The first crystal in each block is a 2 mm long calcite crystal with an extraordinary ( $e$ ) optical axis lying in the  $x$ - $z$  plane,

with an angle of  $\pi/4$  with respect to the  $z$  direction. This crystal generates a spatial mismatch  $g_0$  in the transverse direction  $x$  between the  $H$  and  $V$  polarization components needed for the WM, but also an unwanted temporal walk-off and phase shift, which we compensate with a second 1.1 mm thick cal-

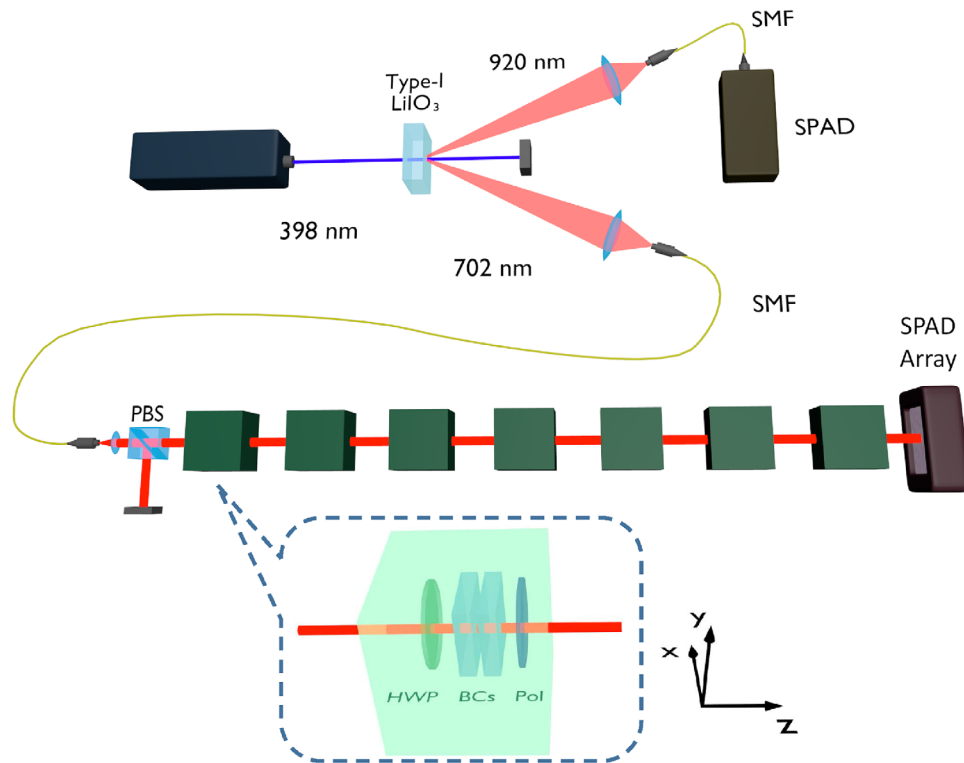


**Figure 3.** Experimental setup. BCs: birefringent crystals. HWP: half-wave plate. LiIO<sub>3</sub>: Lithium Iodate crystal. PBS: polarizing beam-splitter. Pol: polarizer. SMF: single-mode fibre. SPAD: single-photon avalanche diode.

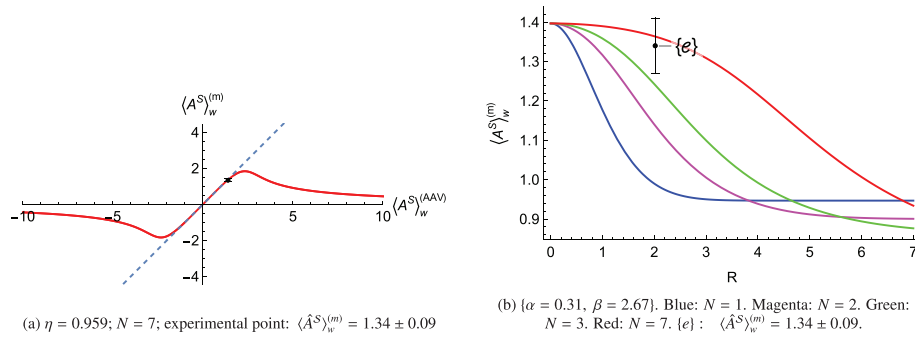


**Figure 4.** Plot (a): Behavior of the measured WV  $\langle \hat{A}^S \rangle_w^{(m)}$  with respect to the one for full pre- and postselection  $\langle \hat{A}^S \rangle_w^{(AAV)}$ , for  $\eta = 0.959$  and  $N = 7$ . The dashed blue line represents the usual WV approximation ( $\eta \rightarrow 1$ ) regime, while the continuous red curve indicates the complete theoretical treatment. As a reference, we report the experimentally-obtained WV and its associated uncertainty ( $\langle \hat{A}^S \rangle_w^{(m)} = 1.34 \pm 0.09$ , respectively indicated by black dot and bars). Plot (b): WV extracted via RWM for  $\{\alpha = 0.31, \beta = 2.67\}$  considering the same measurement resolution power  $R$ , to compare the RWM performances at fixed resolution for different  $N$ . Blue line:  $N = 1$ ; magenta line:  $N = 2$ ; green line:  $N = 3$ ; red line:  $N = 7$ .

cite crystal having the optical  $e$ -axis oriented along the  $y$ -axis. In every block, the interaction Hamiltonian  $\hat{H}_{\text{int}} = g_0(t) \hat{\Pi}_H \otimes \hat{P}_x$  occurs,  $\hat{P}_x$  being the transverse momentum along the  $x$  direction (considering  $z$  the photon propagation direction), since the first birefringent crystal shifts the  $H$  polarization component along  $x$ , thus creating a spatial separation  $g_0 = \int g_0(t) dt$  between the  $H$  and  $V$  components. By rescaling the system in order to have  $g = g_0/2 = 1$ , our evolution operator takes the form  $\hat{U} = \exp(-i\hat{A} \otimes \hat{P})$ .

After the  $N$ th block of the RWM sequence, heralded signal photons are detected with a 2D spatial-resolving single-photon detector prototype, consisting in a  $32 \times 32$  array of “smart pixels,” each hosting a SPAD with dedicated front-end electronics.<sup>[78]</sup> To reduce the SPAD array dark counts contribution, we use the idler photon to gate the device, opening a 6 ns detection window in each pixel SPAD for every heralding count.

The preliminary step of our experiment is to evaluate the behavior of the RWM-extracted WV  $\langle \hat{A}^S \rangle_w^{(m)}$  with respect to  $\langle \hat{A}^S \rangle_w$  for our experimental parameters, i.e.,  $g_0 = 1.48 \pm 0.02$  and  $\sigma_0 = 2.546 \pm 0.001$  (with  $\sigma = 2\sigma_0/g_0$ , giving an interaction intensity parameter  $\eta = 0.959 \pm 0.001$ ), for varying  $\alpha$  and  $\beta$ . The results of this step are reported in **Figure 4a**, showing how our RWM outcome (red continuous curve) would start deviating from the ideal first order approximation (blue dashed line) already for  $|\langle \hat{A}^S \rangle_w^{(m)}| \gtrsim 1.5$ . For this reason, we choose  $\{\alpha = 0.62, \beta = 2.53\}$ , corresponding to the anomalous WV  $\langle \hat{A}^S \rangle_w^{(m)} = 1.35$ , falling in a region still close to the full pre- and postselection case ( $\langle \hat{A}^S \rangle_w = 1.4$ ). **Figure 4b**, instead, lets us appreciate how, for growing  $N$  and a fixed interaction strength, the RWM outcome keeps getting closer to the case of full pre- and postselection of Equation (2).

Our measurement is carried out as follows. First, in order to calibrate the measurement device, we need to find the positions (on the SPAD array) corresponding to the two polarization eigenvalues. This is done by performing two runs with only the birefringent crystals in the optical path of the single photons, and  $|\psi_\alpha\rangle = |H\rangle$  and  $|\psi_\alpha\rangle = |V\rangle$  as input states. Second, we perform the main acquisition, from which the WV will be extracted, with all the optical elements constituting the  $N = 7$  RWM blocks on the signal photons path. Finally, to estimate and eventually compensate for any unwanted spatial shift induced on the photons by polarizers and HWPs, we perform two further acquisitions, one

with only polarizers and HWPs, and one with the optical path completely free.

For each acquisition, the residual dark counts present in the SPAD array output, homogeneously distributed, are properly subtracted. To further reduce the noise and improve the accuracy of our RWM results, the additional dark count contribution due to the SPAD array “hot pixels” (i.e., pixels with a SPAD showing an anomalously large amount of dark counts,<sup>[78]</sup> appearing as anomalous sparse peaks in the device output) is also subtracted by applying a nearest-neighbor smoothing algorithm with a carefully-chosen threshold.

**Figure 5** hosts the photon count distribution obtained for our RWM, from which we obtain, averaging on all photon detec-

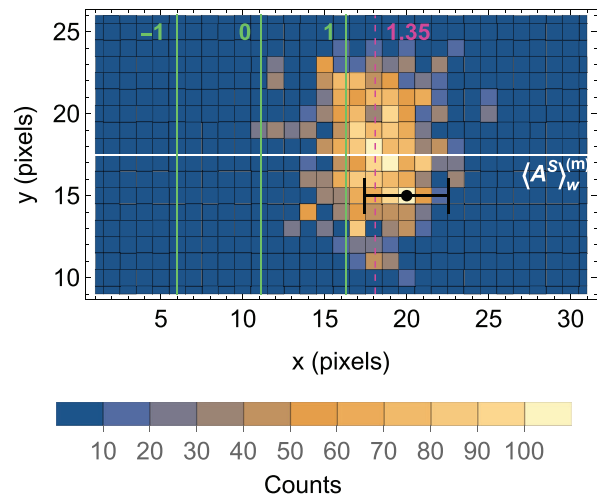


**Figure 5.** Photon detection distribution obtained for the full experimental run with heralded single photons (dark counts subtracted), as a function of the SPAD array pixels in the active region of the sensor (reduced with respect to the original  $32 \times 32$  array, to eliminate dark counts from pixel areas not involved in the RWM). The  $\pm 1$  and 0 green lines indicate, respectively, the borders and the center of the  $\hat{A}^S$  eigenvalues spectrum, while the magenta line at 1.35 highlights the theoretically-expected WV  $\langle \hat{A}^S \rangle_w^{(m)}$ . Conversely, the black dot and bars indicate the WV and associated uncertainty extracted from the first single-photon detection event, i.e.,  $\langle \hat{A}^S \rangle_w^{(m)} = 1.7 \pm 0.4$ .

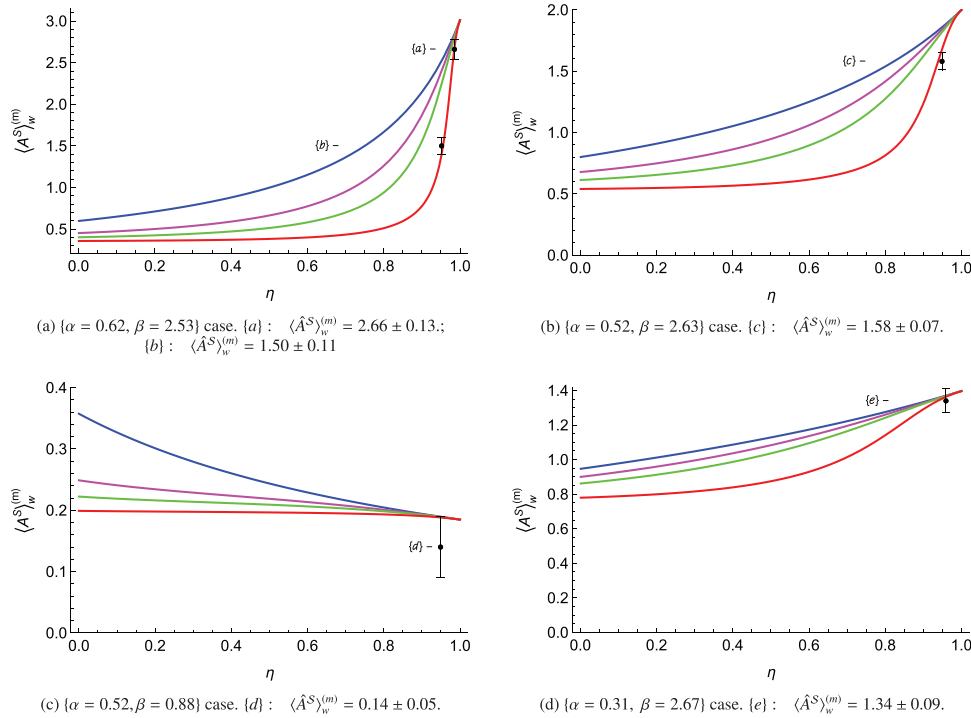


**Figure A1.** Plots (a–d): WV extracted by our RWM procedure for a fixed choice of  $\alpha$  and  $\beta$  (different for each plot), as a function of the interaction intensity parameter  $\eta = \exp\left(-\frac{1}{2\sigma^2}\right)$ . Blue line:  $N = 1$ . Magenta line:  $N = 2$ . Green line:  $N = 3$ . Red line:  $N = 7$ . Dots and uncertainty bars {a–d} in plots (a–c) correspond to the WVs given by the experimental results reported in ref. [73], obtained with different  $\alpha, \beta$  and  $\sigma$  values. Dot and uncertainty bars {e} in plot (d) indicate the WV extracted in the experiment with certified single photons reported in Figure 5.

tion events, the WV  $\langle \hat{A}^S \rangle_w^{(m)} = 1.34 \pm 0.09$ , in good agreement with the theoretically-predicted value  $\langle \hat{A}^S \rangle_w^{(m)} = 1.35$ . Furthermore, from the first heralded photon detection (black dot) we can extract the single-event WV  $\langle \hat{A}^S \rangle_w^{(m)} = 1.7 \pm 0.4$ , where the experimental uncertainty (black horizontal bars) is estimated from the width  $\sigma$  of the initial Gaussian distribution of the single photon. A detailed uncertainty analysis is presented in Appendix B.

## 4. Conclusion

We presented a detailed description of our RWM experimental implementation, showing in detail how, for fixed pre- and postselection states, the precision of the extracted WV  $\langle \hat{A}^S \rangle_w^{(m)}$  scales with the number of blocks (or particles)  $N$ . Our results extend, on the one hand, those already reported in Refs. [36, 37] about the trade-off between the WV measurement resolution (proportional to the weak coupling intensity) and the range of anomalous WVs we are allowed to obtain with no (or eventually small) deviation with respect to the no-entanglement case, in which the WV is described by Equation (2). On the other hand, our results demonstrate the possibility of extracting WVs with reasonably small uncertainty (much below the one achievable with the usual WM protocols) even by detecting a certified single quantum system (in our case, a heralded single photon), strengthening what has been presented in ref. [73] and further highlighting the unprecedented WV extraction capability of the RWM protocol.

The possibility of reliably extracting single-particle anomalous WVs paves the way to a new generation of WV amplification schemes with reduced pointer uncertainty, potentially overcoming the limitations of nowadays WV-based quantum metrology.

## Appendix A: Dependence of the RWM Outcome from $N$

Looking at Equations (5), (12), and (13), we notice that WVs obtained through RWMs depend not only on the coupling intensity and the pre- and postselected state, as usually expected in WM schemes, but also on the number  $N$  of steps implemented in the RWM protocol (or, equivalently, the number of particles in the  $N$ -particles picture).

Indeed, we observe that the WV deviates from the first order approximation prediction as  $\sigma$  decreases (as already observed in ref. [36]), and the larger  $N$ , the stronger this deviation becomes.

This effect does not scale linearly with  $N$ , as can be appreciated from examining Figures A1a,b, where we see the WV extracted by our RWM procedure as a function of the interaction intensity parameter  $\eta = \exp\left(-\frac{1}{2\sigma^2}\right)$ , with  $\eta \rightarrow 1$  corresponding to the case of full pre- and postselection for which Equation (2) holds. The more we stray from the case of complete pre- and postselection, the more the effective coupling causes distortions to the meter distribution, starting with a meter distribution width shrinking around  $\eta \approx 1$ , and, as  $\eta$  decreases, turning the initially Gaussian meter into multi-lobate structures (Figure A2) for growing  $N$ .

As stressed in ref. [36] for  $N = 1$  (i.e., for traditional WMs), the more anomalous the WV, the strongest the meter distortion affecting our  $N = 7$  RWM and, as a consequence, the largest the deviation from the result predicted by Equation (2). For non-anomalous WVs we still observe a slight

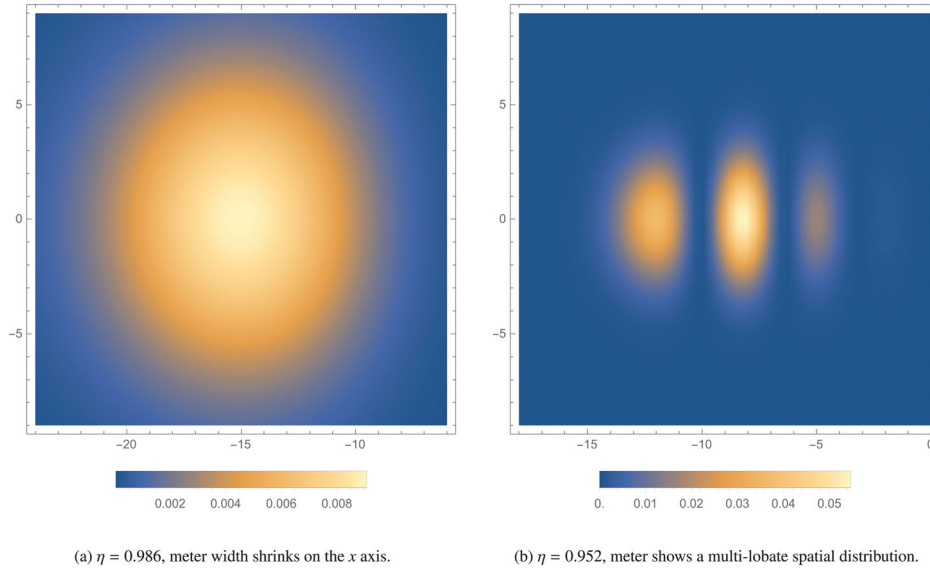


**Figure A2.** Normalized meter distributions ( $x$  and  $y$  axis: arbitrary units) generated by a  $N = 7$  block RWM with  $\{\alpha = 0.62, \beta = 2.53\}$ , for two different interaction intensity parameters  $\eta = \exp\left(-\frac{1}{2\sigma^2}\right)$ . Plot (a), corresponding to a larger  $\eta$  factor, still exhibits a continuous spatial distribution, although quite distorted with respect to the Gaussian one of the initial state  $|\Psi_{in}\rangle$ . Conversely, in plot (b) we can already observe how, for a smaller  $\eta$ , the initially Gaussian-distributed photon end up in the multi-lobate spatial distribution.

deviation with respect to the full pre- and postselection case (Figure A1c), corresponding to a broadening of the meter distribution for decreasing  $\eta$ .

## Appendix B: Experimental Uncertainties Estimation

Here we describe more in detail our method for extracting WVs via RWM, experimental uncertainties included. The first step is the extraction of the Gaussian distribution centroids (along the  $x$  direction)  $q_H$ ,  $q_V$ ,  $q_{pol}$  and  $q_{void}$ , obtained by sending as input states  $|H\rangle$ - and  $|V\rangle$ -photons into the setup in three different configurations: a) with only birefringent crystals; b) with only polarizers and HWPs (“*pol*”); c) with a free optical path (“*void*”). The Gaussian distribution centroids are extracted by performing a linear regression of the acquired data for the states  $|H(V)\rangle$ , averaging over repeated acquisitions. We can, then, extract the WV as

$$\langle \hat{A}^S \rangle_w^{(m)} = \frac{x - x_0}{a} = \frac{2(q - q_{pol} + q_{void}) - q_V - q_H}{q_H - q_V} \quad (B1)$$

where:  $x = q - q_{pol} + q_{void}$  is the position  $q$  of the firing pixel in the SPAD array, corresponding to a detected single photon, corrected for the unwanted spatial deviation induced by the HWP, i.e.,  $q_{pol} - q_{void}$ ;  $x_0 = (q_H + q_V)/2$  is the position corresponding to  $\langle \hat{A}^S \rangle = 0$ ;  $a = (q_H - q_V)/2$  represents the distance (in pixels) between  $\langle \hat{A}^S \rangle = 0$  and the two eigenvalues  $\hat{A}^S = \pm 1$ , providing the conversion factor between the pixel reading on the SPAD array and the polarization WV measured in our RWM. Thus, we can write the uncertainty associated with the extracted WV as

$$\Delta_{\langle \hat{A}^S \rangle_w^{(m)}} = \sqrt{\Delta_A^2 + \Delta_{inhom}^2 + \Delta_\eta^2 + \Delta_{threshold}^2 + \Delta_{angles}^2 + \Delta_{px}^2} \quad (B2)$$

where each term accounts for a different uncertainty contribution, i.e.:

- $\Delta_A$ : statistical uncertainty, estimated with the Monte Carlo method.<sup>[79]</sup>
- $\Delta_{inhom}$ : type-B uncertainty contribution accounting for the inhomogeneities of the birefringent crystals. We evaluate it by estimating the center of the  $V$  photons distribution (the one in principle unaffected by

**Table B1.** Uncertainty budget for our acquisitions.  $\sigma_B$ : total type-B contribution. Coverage factor  $k = 1$ .

	Full run	Single click
$\langle \hat{A}^S \rangle_w^{(m)}$	$1.34 \pm 0.09$	$1.7 \pm 0.4$
$\Delta_A$	0.006	0.4
$\Delta_{inhom}$	0.03	0.03
$\Delta_g$	0.009	0.009
$\Delta_{threshold}$	0.05	0
$\Delta_{angles}$	0.04	0.04
$\Delta_{px}$	0.06	0.06
$\Delta_B$	0.09	0.08
$\Delta_{\langle \hat{A} \rangle_w}$	0.09	0.4

birefringence) both averaging on the photon counts and from a Gaussian fit of the photon counts distribution, eventually evaluating the discrepancies between the results obtained with the two methods.

- $\Delta_\eta$ : type-B contribution related to the uncertainty on the coupling parameter  $\eta$ , which is tied to the uncertainty on  $g_0$ , evaluated by independently estimating  $g_0$  for each birefringent crystal pair and averaging over several calibration runs.
- $\Delta_{threshold}$ : type-B contribution accounting for the threshold chosen for the nearest-neighbor smoothing algorithm exploited to eliminate the dark count contribution to the SPAD array hot pixels. It is estimated as a confidence level on the selected threshold.
- $\Delta_{angles}$ : type-B contribution accounting for the uncertainty on the correct realization of  $\alpha$  and  $\beta$  angles by means of the polarizing plates and HWPs. It is taken as  $1^\circ$ , which we estimate to be the precision we can reach in our RWM experiment.
- $\Delta_{px}$ : type-B contribution due to the SPAD array pixel discretization. We estimate it as the half-size of one pixel.

**Table B1** hosts the uncertainty budget for our acquisition. In the full run, we notice that the dominant contributions are due to the noise-subtraction

procedure, crystals inhomogeneities and  $\alpha, \beta$  angles setting. Conversely, in the single-event estimation the dominant contribution is the statistical one ( $\sigma_A$ ).

## Acknowledgements

This work was financially supported by the projects QuteNoise (call "Trapezio" of Fondazione San Paolo) and AQuTE (MUR, call "PRIN 2022", grant No. 2022RATBS4). The results presented in this article had been achieved also in the context of the following projects: QUID (QUantum Italy Deployment) and EQUO (European QUantum eCOsystems), which are funded by the European Commission in the Digital Europe Programme under the grant agreements number 101091408 and 101091561; QUTEST, which had received funding from the European Union's Horizon Europe under the grant agreement number 101113901. This work was also funded by the project 23NRM04 NoQTeS, that received funding from the European Partnership on Metrology, co-financed from the European Union's Horizon Europe Research and Innovation Programme and by the Participating States. This project received funding also from the European Union's Horizon Europe research and innovation programme under grant agreement No. 101178170, and from the Israel Science Foundation under grants No. 2689/23 and No. 2208/24.

## Conflict of Interest

The authors declare no conflict of interest.

## Data Availability Statement

The data that support the findings of this study are available from the corresponding author upon reasonable request.

## Keywords

weak measurements, weak values, single photons

Received: September 27, 2024

Revised: March 17, 2025

Published online: April 29, 2025

- [1] Y. Aharonov, D. Z. Albert, L. Vaidman, *Phys. Rev. Lett.* **1988**, *60*, 1351.
- [2] B. Tamir, E. Cohen, *Quanta* **2013**, *2*, 7.
- [3] N. Ritchie, J. Story, R. Hulet, *Phys. Rev. Lett.* **1991**, *66*, 1107.
- [4] O. Hosten, P. Kwiat, *Science* **2008**, *319*, 787.
- [5] M. Hallaji, A. Feizpour, G. Dmochowski, J. Sinclair, A. Steinberg, *Nat. Phys.* **2017**, *13*, 540.
- [6] F. Piacentini, A. Avella, M. P. Levi, R. Lussana, F. Villa, A. Tosi, F. Zappa, M. Gramegna, G. Brida, I. P. Degiovanni, M. Genovese, *Phys. Rev. Lett.* **2016**, *116*, 180401.
- [7] L. Zhou, Y. Turek, C. Sun, F. Nori, *Phys. Rev. A* **2014**, *88*, 053815.
- [8] A. Avella, F. Piacentini, M. Borsarelli, M. Barbieri, M. Gramegna, R. Lussana, F. Villa, A. Tosi, I. P. Degiovanni, M. Genovese, *Phys. Rev. A* **2017**, *96*, 052123.
- [9] W. W. Pan, X.-Y. Xu, Y. Kedem, Q.-Q. Wang, Z. Chen, M. Jan, K. Sun, J.-S. Xu, Y.-J. Han, C.-F. Li, G.-C. Guo, *Phys. Rev. Lett.* **2019**, *123*, 150402.
- [10] J. Lundeen, B. Sutherland, A. Patel, C. Stewart, C. Bamber, *Nature* **2011**, *474*, 188.
- [11] M. Goggin, M. P. Almeida, M. Barbieri, B. P. Lanyon, J. L. O'Brien, A. G. White, G. J. Pryde, *Proc. Natl. Acad. Sci. USA* **2011**, *108*, 1256.
- [12] F. Piacentini, A. Avella, M. P. Levi, M. Gramegna, G. Brida, I. P. Degiovanni, E. Cohen, R. Lussana, F. Villa, A. Tosi, F. Zappa, M. Genovese, *Phys. Rev. Lett.* **2016**, *117*, 170402.
- [13] G. Thekkadath, L. Giner, Y. Chalich, M. J. Horton, J. Banker, J. S. Lundeen, *Phys. Rev. Lett.* **2016**, *117*, 120401.
- [14] F. Piacentini, A. Avella, E. Rebufello, R. Lussana, F. Villa, A. Tosi, M. Gramegna, G. Brida, E. Cohen, L. Vaidman, I. P. Degiovanni, M. Genovese, *Nat. Phys.* **2017**, *13*, 1191.
- [15] E. Rebufello, F. Piacentini, A. Avella, R. Lussana, F. Villa, A. Tosi, M. Gramegna, G. Brida, E. Cohen, L. Vaidman, I. P. Degiovanni, M. Genovese, *Appl. Sci.* **2021**, *11*, 4260.
- [16] M. W. Chen, O. Young, M. Schlosshauer, M. Beck, *Phys. Rev. A* **2023**, *108*, 022420.
- [17] M. Schlosshauer, *Phys. Rev. A* **2024**, *110*, 032215.
- [18] L. Vaidman, A. Ben-Israel, J. Dziejwior, L. Knips, M. Weiß, J. Meinecke, C. Schwemmer, R. Ber, H. Weinfurter, *Phys. Rev. A* **2017**, *96*, 032114.
- [19] O. Calderón-Losada, T. T. M. Quistian, H. Cruz-Ramirez, S. Murgueitio Ramirez, A. B. U'Ren, A. Botero, A. Valencia, *Commun. Phys.* **2020**, *3*, 117.
- [20] V. V. Vorobyov, J. Meinel, H. Sumiya, S. Onoda, J. Isoya, O. Gulinsky, J. Wrachtrup, *Phys. Rev. A* **2023**, *107*, 042212.
- [21] S. Virzi, E. Rebufello, F. Atzori, A. Avella, F. Piacentini, R. Lussana, I. Cusini, F. Madonini, F. Villa, M. Gramegna, E. Cohen, I. P. Degiovanni, M. Genovese, *Quantum Sci. Technol.* **2024**, *9*, 045027.
- [22] Y. W. Cho, H. T. Lim, Y. S. Ra, Y. H. Kim, *New J. Phys.* **2010**, *12*, 023036.
- [23] G. Bizzarri, S. Gherardini, M. Manrique, F. Bruni, I. Gianani, M. Barbieri, *arXiv:2406.06713* **2024**.
- [24] M. Tukiainen, H. Kobayashi, Y. Shikano, *Phys. Rev. A* **2017**, *95*, 052301.
- [25] K. Siva, G. Koolstra, J. Steinmetz, W. P. Livingston, D. Das, L. Chen, J. M. Kreikebaum, N. Stevenson, C. Jünger, D. I. Santiago, I. Siddiqi, A. N. Jordan, *PRX Quantum* **2023**, *4*, 040324.
- [26] R. Vijay, C. Macklin, D. H. Slichter, S. J. Weber, K. W. Murch, R. Naik, A. N. Korotkov, I. Siddiqi, *Nature* **2012**, *490*, 77.
- [27] S. J. Weber, A. Chantasri, J. Dressel, A. N. Jordan, K. W. Murch, I. Siddiqi, *Nature* **2014**, *511*, 570.
- [28] P. Dixon, D. Starling, A. Jordan, J. Howell, *Phys. Rev. Lett.* **2009**, *102*, 173601.
- [29] J. Howell, D. Starling, B. Dixon, P. Vudyaasetu, A. Jordan, *Phys. Rev. A* **2010**, *81*, 033813.
- [30] X. Xu, Y. Kedem, K. Sun, L. Vaidman, C. Li, G. Guo, *Phys. Rev. Lett.* **2013**, *111*, 033604.
- [31] G. Strübi, C. Bruder, *Phys. Rev. Lett.* **2013**, *110*, 083605.
- [32] G. Jayaswal, G. Mistura, M. Merano, *Opt. Lett.* **2014**, *39*, 6257.
- [33] O. M. Loaiza, M. Mirhosseini, B. Rodenburg, R. Boyd, *Phys. Rev. Lett.* **2014**, *112*, 200401.
- [34] J. Sinclair, M. Hallaji, A. Steinberg, J. Tollaksen, A. Jordan, *Phys. Rev. A* **2017**, *96*, 052128.
- [35] A. Jordan, J. Martínez-Rincón, J. Howell, *Phys. Rev. X* **2014**, *4*, 011031.
- [36] F. Piacentini, A. Avella, M. Gramegna, R. Lussana, F. Villa, A. Tosi, G. Brida, I. P. Degiovanni, M. Genovese, *Sci. Rep.* **2018**, *8*, 6959.
- [37] J. Dziejwior, L. Knips, D. Farfurnik, K. Senkalla, N. Benshalom, J. Efroni, J. Meinecke, S. Bar-Ad, H. Weinfurter, L. Vaidman, *Proc. Natl. Acad. Sci. USA* **2019**, *116*, 2881.
- [38] S. Pang, J. Dressel, T. Brun, *Phys. Rev. Lett.* **2014**, *113*, 030401.
- [39] M. Asano, K. Y. Bliokh, Y. P. Bliokh, A. G. Kofman, R. Ikuta, T. Yamamoto, Y. S. Kivshar, L. Yang, N. Imoto, S. K. Ozdemir, F. Nori, *Nat. Commun.* **2016**, *7*, 13488.
- [40] W. Liu, J. Martínez-Rincón, G. Viza, J. Howell, *Opt. Lett.* **2017**, *42*, 903.
- [41] G. Foletto, L. Calderaro, A. Tavakoli, M. Schiavon, F. Picciariello, A. Cabello, P. Villorosi, G. Vallone, *Phys. Rev. Applied* **2020**, *13*, 044008.
- [42] G. Foletto, L. Calderaro, G. Vallone, P. Villorosi, *Phys. Rev. Res.* **2020**, *2*, 033205.

- [43] G. Foletto, M. Padovan, M. Avesani, H. Tebyanian, P. Villorresi, G. Vallone, *arXiv:2101.12074* **2021**.
- [44] L. J. Salazar-Serrano, D. A. Guzmán, A. Valencia, J. P. Torres, *Opt. Expr.* **2015**, *23*, 10097.
- [45] M. Iinuma, Y. Suzuki, G. Taguchi, Y. Kadoya, H. F. Hofmann, *New J. Phys.* **2011**, *13*, 033041.
- [46] J. Z. Salvail, M. Agnew, A. S. Johnson, E. Bolduc, J. Leach, R. W. Boyd, *Nat. Photon.* **2013**, *7*, 316.
- [47] V. Gebhart, K. Snizhko, T. Wellens, A. Buchleitner, A. Romito, Y. Gefen, *Proc. Natl. Acad. Sci. USA* **2020**, *117*, 5706.
- [48] Y. Kim, S. Y. Yoo, Y. H. Kim, *Phys. Rev. Lett.* **2022**, *128*, 040503.
- [49] Y. W. Cho, Y. Kim, Y.-H. Choi, Y.-S. Kim, S.-W. Han, S.-Y. Lee, S. Moon, Y.-H. Kim, *Nat. Phys.* **2019**, *15*, 665.
- [50] G. I. Viza, J. Martínez-Rincón, W. T. Liu, J. Howell, *Phys. Rev. A* **2016**, *94*, 043825.
- [51] X. X. Peng, P. Yin, W.-H. Zhang, G.-C. Li, D.-Y. He, X.-Y. Xu, J.-S. Xu, G. Chen, C.-F. Li, G.-C. Guo, *Opt. Expr.* **2020**, *28*, 19629.
- [52] V. Cimini, I. Gianani, F. Piacentini, I. P. Degiovanni, M. Barbieri, *Quantum Sci. Technol.* **2020**, *5*, 025007.
- [53] J. Huang, Y. Li, C. Fang, H. Li, G. Zeng, *Phys. Rev. A* **2019**, *100*, 012109.
- [54] A. Leggett, *Phys. Rev. Lett.* **1989**, *62*, 2325.
- [55] A. Peres, *Phys. Rev. Lett.* **1989**, *62*, 2326.
- [56] I. Duck, P. Stevenson, E. Sudarshan, *Phys. Rev. D* **1989**, *40*, 2112.
- [57] Y. Aharonov, L. Vaidman, *Phys. Rev. Lett.* **1989**, *62*, 2327.
- [58] C. Ferrie, J. Combes, *Phys. Rev. Lett.* **2014**, *112*, 040406.
- [59] C. Ferrie, J. Combes, *Phys. Rev. Lett.* **2014**, *113*, 120404.
- [60] M. Pusey, *Phys. Rev. Lett.* **2014**, *113*, 200401.
- [61] J. R. Hance, M. Ji, H. F. Hofmann, *New J. Phys.* **2023**, *25*, 113028.
- [62] J. Dressel, *Phys. Rev. A* **2015**, *91*, 032116.
- [63] L. Vaidman, *J. of Phys. A: Math. and Th.* **2015**, *48*, 465303.
- [64] K. Lyons, J. Dressel, A. Jordan, J. Howell, P. Kwiat, *Phys. Rev. Lett.* **2015**, *114*, 170801.
- [65] G. Knee, J. Combes, C. Ferrie, E. Gauger, *Quantum Meas. Quantum Metrol.* **2016**, *3*, 32.
- [66] D. Mundarain, M. Orszag, *Phys. Rev. A* **2016**, *93*, 032106.
- [67] L. Vaidman, *Philos. T. Roy. Soc. A* **2017**, *375*, 2106.
- [68] R. Kastner, *Found. Phys.* **2017**, *47*, 697.
- [69] E. Cohen, *Found. Phys.* **2017**, *47*, 1261.
- [70] L. Diósi, *Phys. Rev. A* **2016**, *94*, 010103.
- [71] A. A. Abbott, R. Silva, J. Wechs, N. Brunner, C. Branciard, *Quantum* **2019**, *3*, 194.
- [72] J. Zhou, L. C. Kwek, J. L. Chen, *arXiv:2303.17081*, **2023**.
- [73] E. Rebuffello, F. Piacentini, A. Avella, M. A. de Souza, M. Gramegna, J. Dziewior, E. Cohen, L. Vaidman, I. P. Degiovanni, M. Genovese, *Light: Sci. & Appl.* **2021**, *10*, 106.
- [74] A. Avella, I. R. Berchera, I. P. Degiovanni, G. Brida, M. Genovese, *Opt. Lett.* **2016**, *41*, 1841.
- [75] L. Vaidman, A. Ben-Israel, J. Dziewior, L. Knips, M. Weißl, J. Meinecke, C. Schwemmer, R. Ber, H. Weinfurter, *Phys. Rev. A* **2017**, *96*, 032114.
- [76] Y. Aharonov, D. Z. Albert, A. Casher, L. Vaidman, *Phys. Lett. A* **1987**, *124*, 199.
- [77] E. Rebuffello, F. Piacentini, M. López, R. A. Kirkwood, I. R. Berchera, M. Gramegna, G. Brida, S. Kück, C. J. Chunnillall, M. Genovese, I. P. Degiovanni, *Metrologia* **2019**, *56*, 025004.
- [78] F. Villa, R. Lussana, D. Bronzi, S. Tisa, A. Tosi, F. Zappa, A. D. Mora, D. Contini, D. Durini, S. Weyers, W. Brockherde, *IEEE J. Sel. Top. Quantum Electron.* **2014**, *20*, 364.
- [79] JCGM 2008 Evaluation of Measurement Data-Supplement 1 to the "Guide to the Expression of Uncertainty in Measurement" - Propagation of distributions using a Monte Carlo method JCGM 101:2008.